Asian Journal of Chemistry; Vol. 37, No. 3 (2025), 543-551

ASIAN JOURNAL OF CHEMISTRY

https://doi.org/10.14233/ajchem.2025.33120

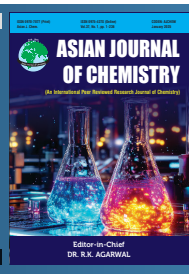

Molecular Docking, Computational DFT, Biological Activity, Phytochemical Analysis and Spectrum Analysis Investigations of Neoandrographolide

P. KAMALARAJAN[1,*], J. IRSHAD AHAMED[2], S. RAMESH[1] and M.F. VALAN[3]

[1]Department of Chemistry, R.M.D. Engineering College, Kavaraipettai-601206, India
[2]Department of Chemistry, Theivanai Ammal College for Women, Villupuram-605401, India
[3]Department of Chemistry, Loyola College, University of Madras, Chennai-600034, India

*Corresponding author: E-mail: rajanfx@gmail.com

Received: 2 December 2024; *Accepted*: 25 January 2025; *Published online*: 28 February 2025; AJC-21909

In this work, neoandrographolide ($C_{26}H_{40}O_8$) was isolated first time from the ethanolic extract of Nilavembu Kudineer Chooranam (NKC), traditional Siddha medicine powder. Thin-layer chromatographic (TLC), GC-MS and mass spectrometry techniques were employed to extract after the preliminary phytochemical screening. Neoandrographolide has a significant level of α-amylase inhibition activity. The *ab initio* DFT theory of DFT-B3LYP/6-311++ G(d,p) basis set technique was used for theoretical studies and comparison with the three experimental spectral studies such as ^{1}H, ^{13}C NMR, FTIR and UV-visible methods. When compared to the theoretical computational density functional theory (DFT) using Gaussian 9.0, the results have shown that the investigated compounds are potential therapeutic leads for *in vitro* biological and *in silico* molecular docking utilizing auto dock vina 4.2. Based on the results, it is confirmed that compound neoandrographolide would be most effective against α-amylase inhibitor activities.

Keywords: Neoandrographolide, Nilavembu Kudineer Chooranam, Molecular docking.

INTRODUCTION

The constituents of nine plants ingredients in the Nilavembu Kudineer Chooranam (NKC) herbal formulation and its synergistic effects are already reported in the literature [1]. In comparison to synthetic drugs, herbal therapy is more economical, exhibits fewer adverse effects and additionally bolsters the immune system while promoting spontaneous recovery, thus, maintaining a healthy metabolism and hormones. Most herbal remedies have a wide range of therapeutic uses [2,3]. Plant-derived substances can be classified into essential groups such as terpenoids, alkaloids, phenyl prostanoids and related phenolic compounds based on their metabolic sources. NKC is recommended in Siddha medicine to treat and prevent fevers and viral infections. Additionally, it is crucial for the body's fight against chikungunya and dengue. The components of Kudineer have hepatoprotective, anti-inflammatory, antimicrobial, analgesic, antioxidant, antiviral, cytotoxic and antidiabetic activities [4].

Previous work on *Andrographis paniculata* revealed that the neoandrographolide possessed biological characteristics such as chemosensitizing, hypolipidemic actions [5-7], anti-inflammatory and antiviral properties [8,9]. This compound contains biologically active compounds such as andrographolide [10], β-vetivenene [11], α-zingiberene [12] and α-santalol [13].

To our best of knowledge, no literature exists about the separation of neoandrographolide from NKC, and also no studies on DFT, molecular docking, biological activity or α-amylase inhibitor efficacy is reported. To isolate and characterize neoandrographolide from NKC and assess its capacity to inhibit α-amylase activity studies, this work was undertaken. Moreover, the preliminary phytochemical analysis of ethanolic extract of NKC, chromatographic analysis (TLC), gas chromatogram mass spectrometric (GCMS) analysis, the *in silico* and DFT computational studies were also carried out.

EXPERIMENTAL

Phytochemical screening: A standard procedure [14] was applied to conduct a phytochemical study of the ethanolic extract of Nilavembu Kudineer Chooranam in order to determine the

presence of alkaloids, flavonoids, phenols, tannins, coumarin, terpenoids and glycosides.

TLC analysis: Neoandrographolide was subjected to thin-layer chromatography (TLC) analysis using a TLC cutter and silica gel $60F_{254}$. TLC plates with glass capillaries detected the extract. The TLC chamber solvents were butanol, acetic acid, and water. After 30 min of pre-saturation with the mobile phase, the plates were retained in the chamber and eluted using the solvent system. The plate was sprayed with multiple spray reagents, dried and visually evaluated in a UV room after elution.

GC-MS analysis: The GC-MS analysis of ethanolic extract of NKC in EI mode was performed on the Shimadzu QP2020. The split sampling method involved injecting the sample at a 1:10 ratio and the oven was maintained at 280 ºC at 10 ºC/min. The retention indices (RI) of the molecule were calculated by equating the retention durations of a sequence. Each component was identified by comparing the maintenance index of each component to data from the literature. Identifications in the NIST collection were linked to the spectrum of the unidentified components. The molecular weights, names, chemical structures and formulas of the test materials were determined [15].

Column chromatography: The ethanolic extract of NKC was diluted with methanol before being adsorbed on 100-200 mesh silica gel. Once the solvent has evaporated, the sample was inserted onto a silica gel column containing hexane and mesh size of 100 to 200. The polarity was developed by adding varying hexane to ethyl acetate ratios and 100% ethyl acetate after hexane was eluted in the column. Ethyl acetate: 100% chloroform and chloroform in the ratios 90:10, 80:20, 70:30, 60:40, 50:50, 40:60, 30:70 and 20:80 were then entirely eluted in the column. Once more methanol was used to elute the column (98:2; 96:4; 94:2; 92:8; 90:10; 85:15; 80:20). One hundred and eighteen fractions in all were collected and under close inspection with TLC. Fractions between 64 and 78 revealed similar fractions. As the pressure dropped, the solvent evaporated and the fractions combined. The raw ingredients of final product were purified using hot ethanol and activated charcoal and the fractions were set aside for crystallization. The resultant solid was analyzed using mass spectra, FT-IR and ^{1}H NMR.

Analytical data of isolated compound: The colourless needle shape crystal, m.p.: 162-164 ºC; $C_{26}H_{40}O_8$;; FT-IR (KBr, ν_{max}, cm^{-1}): 3449, 2940, 2847, 1748, 1609, 1457, 1353 and 910. LC-Mass: *m/z* 480.59 (MH^+) HRMS and molecular ion peak for water molecule at *m/z* 498.56 $(M+H+H_2O)^+$; ^{1}H NMR δ ppm: 0.61 (3H, s), 0.84-0.87 (1H, m), 0.95 (3H, s), 1.01-1.03 (1H, m), 1.19-1.21 (1H, m), 1.26-1.31 (1H, m), 1.37-1.40 (1H, m), 1.48-1.55 (2H, m), 1.61-1.64 (1H, d), 1.70-1.72 (2H, m), 1.76-1.78 (1H, d), 1.82-1.84 (1H, d), 1.89-1.93 (1H, m), 1.98-2.01 (1H, m), 2.24-2.28 (1H, m), 2.33-2.36 (1H, m), 2.90-2.94 (1H, m), 3.01-3.12 (4H, m), 3.39-3.43 (1H, m), 3.62-3.65 (1H, m), 3.87-3.89 (1H, d), 4.01-4.03 (1H, d), 4.37-4.40 (1H, t), 4.59 (1H, s), 4.79-4.86 (6H, m), 7.47 (1H, s). This pattern of the spectrum is to identify an isolated neoandrographolide.

Computational details: Gaussian 09 [16-18] was used as a software package for gradient geometry optimization and *ab initio* molecular simulations with basis set of DFT [19-21]. The scaling factor of 0.9613 must exhibit considerably better agreement with observational data [22-24]. The GIAO technique was used to estimate the chemical shifts for NMR results [25]. The investigations of chemical reactivity and Mulliken charges were performed to elucidate the energy of (HOMO-LUMO).

In vitro analysis

Antibacterial activity: For the antibacterial assay, the bacterial strains employed were *Proteus mirabilis* (MTCC 1771), *Staphylococcus aureus* (MTTC 3615), *Enterococcus faecalis* (MTCC 439) and *Yersinia enterocolitica* (MTCC 840). The Mueller-Hinton broth, having a pH 7.0, yielded Gram-negative bacteria, while the nutrient-rich broth resulted in Gram-positive bacteria. The cultures underwent a 24 h incubation period at 37 ºC in a rotator shaker. Sterile 6 mm discs were filled and neoandrographolide (25 mL) was added. The discs were then left to soak for 10 to 15 min. After that, they were incubated and then stored at 37 ºC for 24 h. The zone of inhibition (mm) of the compound was assessed using the pathogenic bacteria index one day later. The Mean ± SD data were displayed and each study was conducted in three copies.

In vitro antioxidant study

Hydrogen peroxide (H_2O_2) scavenging activity: The H_2O_2 scavenging test was determined using reported methodology [26,27]. In brief, 0.6 mL of H_2O_2 solution was mixed with neoandrographolide dissolved in ethanol at different concentration of 1 mg/mL (10-50 mg/mL). After incubating for 15 min, the absorbing capacity of the chemical reaction at 230 nm. The pure, undiluted H_2O_2 is called a "blank solution."

α-Amylase assay: The inhibitory activity of α-amylase in the test samples was assessed using a modified standard method. The volume of test samples, standard (acarbose) and control (no standard/test samples) were increased to 100 µL α-amylase solution (0.1 mg/mL) and incubated for 15 min at 37 ºC followed by the addition of 100 µL of starch solution. Following a 1 h incubation period at 37 ºC, 10 µL of 1 M HCl and 100 µL of iodine reagent were added to the test tubes containing the mixture. The absorbance of the mixture was measured at 580 nm.

***In silico* molecular docking and computational studies:** The docking study was carried out using Autodock 4.2. Rigid receptors and flexible ligands were used to perform docking investigations. The protein file was selected for the docking study of the isolated compound neoandrographolide. The FAT10's X-ray crystal structure was developed (RSCB PDB code: 2MBE). Molecular docking experiments were able to target the FAT10 protein successfully. The binding site was determined by grid box size and grid box. The grid spacing value for protein was found to be 0.375 Å. Chem Draw 12.0 was used to display the structure of neoandrographolide ligand. The mol format was used to transform the 2D compound structures. The Auto Dock application was then used to further turn it into a 3D structure [28]. Auto Dock ligand input tools were used to create and purify this ligand. The application Discovery Studio generated the visualization results, and the final refined ligands were acquired as pdbqt files for subsequent molecular docking studies *via* output-save [29].

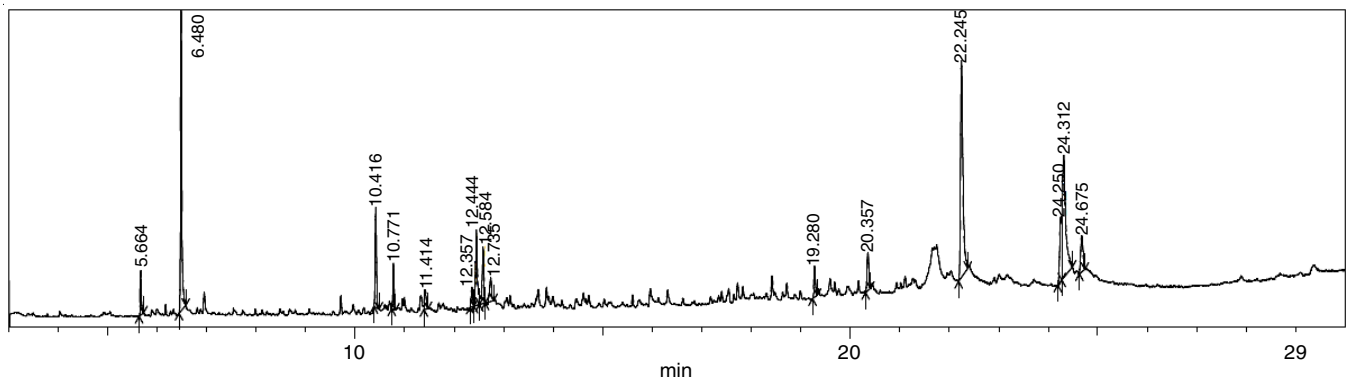

Fig. 1. Chromatogram of ethanolic extract of Nilavembu Kudineer Chooranam (NKC)

RESULTS AND DISCUSSION

The TLC study was performed using acetic acid:butanol: water (1:4:2) mobile phase for the analysis of neoandrographolide. The results under UV light at 254 nm confirmed the presence of one ingredient in neoandrographolide with R_f value of 0.66.

GC-MS analysis of ethanolic extracted NKC: Acids, alcohols, hydrocarbon and other substances can have their components identified using the GC-MS method using the molecular formula, peak area and retention time to identify the phytochemical compounds. The peak area of active principles as a percentage, molecular structure are all shown in the GC-MS spectrum of the ethanolic extraction ofNKC (Fig. 1).

Optimized geometrical parameters: The resulting theoretical deductions (SDD) are in good agreement with the known structural properties of similar derivatives. Fig. 2 illustrates the optimized structure of neoandrographolide. Their ideal step numbers, which obtained from the possible energy measurement curves, as shown in Fig. 3. As shown in Tables 1 and 2, the bond lengths and angles of the optimized structure were determined by the DFT approach. Employing B3LYP/6-311G ++(d,p), the optimized structure NAG derived least energy is -1616.5093 a.u. The computations will determine the optimal shape for NAG to lower the potential energy surface. The bond lengths (C9-C18) and (C14-C15) are aromatic and show signs of double bonds. On the other hand, certain bonds resemble a single bond. The bond lengths and angles of the molecular structure were ascertained by applying this geometry. The bond distance for the carbonyl group of C16–O67) and hydrogen bond is found to be 1.22 Å and 1.94 Å, respectively. In this compound, the NAG-optimized length of hydrogen bond distance is less than 2 Å. Hence, this molecule will possess excellent biological activity. The hydrogen bonds containing bonds such as (C21-O69-H47) and (O68-H47-O69) have the values of bond angles 100.20º and 140.10º, respectively.

Vibrational analysis: The key FTIR data of isolated molecule of theoretical and experimental results are displayed in Table-3. The OH stretching frequency peak values at 3486 and 3437 cm^{-1} found in the theoretical and literature agreed with the stretching bond peaks at 3449 cm^{-1} (-OH group) in the experimental FTIR spectrum. The experimental CH stretching vibration value of 2940 cm^{-1} (=CH stretch) is nearly in line

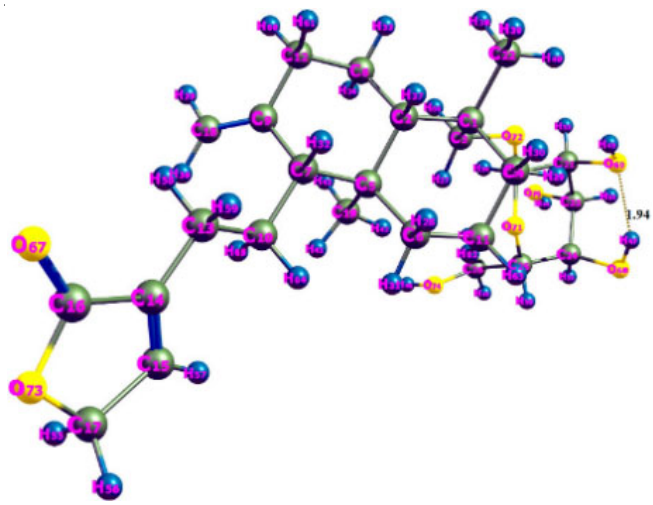

Fig. 2. Optimized geometry (SDD) of neoandrographolide

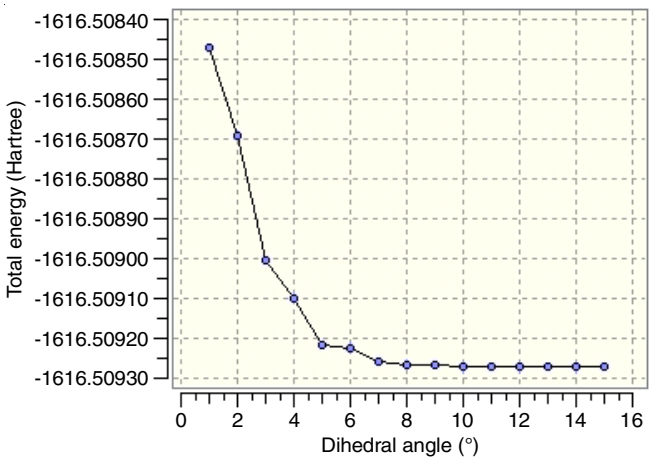

Fig. 3. Potential energy curve using DFT/B3LYP method with 6-311 ++G (d,p) basis set for neoandrographolide

with the theoretical and literature CH stretching vibration peak values of 2993 and 2934 cm^{-1}, respectively. The (-CH_3) asymmetric stretching frequency can be determined by the value of 2847 cm^{-1}, which corresponds to the theoretical and literature -CH_3 asymmetric stretch vibration values of 2839 and 2840 cm^{-1}, respectively. The additional vibration modes found in this investigation were those of the experimental carbonyl group (C=O) stretching band is identified at 1609 cm^{-1} and the =CH

TABLE-1
CALCULATED BOND LENGTHS (Å) OF THE NEOANDROGRAPHOLIDE MOLECULE WITH DFT THEORY EMPLOYING 6-311G++(d,p) BASIS SET

Atom number	B3LYP/6-311G++(d,p)	Atom number	B3LYP/6-311G++(d,p)	Atom number	B3LYP/6-311G++(d,p)
C1-C2	1.58	C9-C18	1.34	C20-H54	1.09
C1-C3	1.54	C10-C13	1.54	C20-O71	1.45
C1-C4	1.55	C10-H64	1.09	C20-O72	1.42
C1-C22	1.55	C10-H65	1.09	C21-C23	1.53
C2-C5	1.59	C11-H62	1.09	C21-H53	1.09
C2-C8	1.55	C11-H63	1.09	C21-O69	1.46
C2-H37	1.10	C12-H60	1.09	C22-H38	1.09
C3-H27	1.08	C12-H61	1.10	C22-H39	1.09
C3-H66	1.09	C13-C14	1.50	C22-H40	1.09
C3-O72	1.48	C13-H58	1.09	C23-C24	1.54
C4-C11	1.53	C13-H59	1.10	C23-H52	1.09
C4-H29	1.09	C14-C15	1.34	C23-O70	1.47
C4-H30	1.10	C14-C16	1.49	C24-C25	1.54
C5-C6	1.55	C15-C17	1.50	C24-H51	1.09
C5-C7	1.60	C15-H57	1.08	C24-O68	1.45
C5-C19	1.55	C16-O67	1.22	C25-C26	1.52
C6-C11	1.54	C16-O73	1.41	C25-H50	1.09
C6-H28	1.10	C17-H55	1.09	C25-O71	1.47
C6-H31	1.09	C17-H56	1.09	C26-H48	1.10
C7-C9	1.53	C17-O73	1.47	C26-H49	1.09
C7-C10	1.55	C18-H35	1.08	C26-O74	1.46
C7-H32	1.10	C18-H36	1.08	H44-O70	0.97
C8-C12	1.54	C19-H41	1.09	H44-O70	0.98
C8-H33	1.09	C19-H42	1.09	H46-O74	0.97
C8-H34	1.09	C19-H43	1.09	H47-O68	0.98
C9-C12	1.51	C20-C21	1.53	H47-O69	1.94

TABLE-2
CALCULATED BOND ANGLES (º) OF THE NEOANDROGRAPHOLIDE MOLECULE WITH DFT THEORY EMPLOYING 6-311G++(d,p) BASIS SET

Atom number	B3LYP/6-311G++(d,p)	Atom number	B3LYP/6-311G++(d,p)	Atom number	B3LYP/6-311G++(d,p)
C2-C1-C3	111.50	C11-C6-H31	108.90	H35-C18-H36	115.80
C2-C1-C4	109.00	C6-C11-H62	110.90	H41-C19-H42	106.50
C2-C1-C22	109.40	C6-C11-H63	109.10	H41-C19-H43	107.00
C1-C2-C5	117.20	H28-C6-H31	106.70	H42-C19-H43	108.30
C1-C2-C8	114.00	C9-C7-C10	114.10	C21-C20-H54	111.00
C1-C2-H37	102.80	C9-C7-H32	106.40	C21-C20-O71	110.60
C3-C1-C4	110.90	C7-C9-C12	113.30	C21-C20-O72	106.70
C3-C1-C22	108.40	C7-C9-C18	125.30	C20-C21-C23	111.00
C1-C3-H27	111.90	C10-C7-H32	106.40	C20-C21-H53	109.70
C1-C3-H66	110.80	C7-C10-C13	112.70	C20-C21-O69	109.10
C1-C3-O72	109.60	C7-C10-H64	109.40	H54-C20-O71	110.40
C4-C1-C22	107.60	C7-C10-H65	110.40	H54-C20-O72	111.50
C1-C4-C11	114.10	C12-C8-H33	108.80	H71-C20-O72	106.50
C1-C4-H29	108.80	C12-C8-H34	108.90	C20-O71-C25	116.10
C1-C4-H30	107.70	C8-C12-C9	111.20	C23-C21-H53	109.80
C1-C22-H38	112.40	C8-C12-H60	110.30	C23-C21-O69	106.80
C1-C22-H39	110.40	C8-C12-H61	108.50	C21-C23-C24	111.80
C1-C22-H40	110.00	H33-C8-H34	106.70	C21-C23-H52	108.90
C5-C2-C8	111.50	C12-C9-C18	121.30	C21-C23-O70	105.20
C5-C2-H37	103.80	C9-C12-H60	110.50	H53-C21-O69	110.40
C2-C5-C6	108.30	C9-C12-H61	109.30	C21-O69-H45	107.80
C2-C5-C7	105.90	C9-C18-H35	120.90	C21-O69-H47	100.20
C2-C5-C19	114.80	C9-C18-H36	123.30	H38-C22-H39	108.30
C8-C2-H37	106.00	C13-C10-H64	108.10	H38-C22-H40	107.30
C2-C8-C12	111.20	C13-C10-H65	109.70	H39-C22-H40	108.20
C2-C8-H33	110.20	C10-C13-C14	114.70	C24-C23-H52	108.60
C2-C8-H34	110.90	C10-C13-H58	110.60	C24-C23-O70	111.30
H27-C3-H66	109.80	C10-C13-H59	109.50	C23-C24-C25	112.80

H27-C3-O72	107.50	H64-C10-H65	106.40	C23-C24-H51	109.30
H66-C3-O72	107.00	H62-C11-H63	105.80	C23-C24-O68	109.00
C3-O72-C20	114.70	H60-C12-H61	107.00	H52-C23-O70	111.00
C11-C4-H29	110.10	C14-C13-H58	108.60	C23-O70-H44	110.60
C11-C4-H30	109.00	C14-C13-H59	108.20	C25-C24-H51	109.20
C4-C11-C6	111.50	C13-C14-C15	131.10	C25-C24-O68	110.70
C4-C11-H62	110.00	C13-C14-C16	120.40	C24-C25-C26	114.80
C4-C11-H63	109.30	H58-C13-H59	104.80	C24-C25-H50	107.60
H29-C4-H30	106.90	C15-C14-C16	108.50	C24-C25-O71	109.80
C6-C5-C7	109.60	C14-C15-C17	110.50	H51-C24-O68	105.60
C6-C5-C19	109.30	C14-C15-57	127.00	C24-O68-H47	108.00
C5-C6-C11	113.50	C14-C16-O67	129.60	C26-C25-H50	108.20
C5-C6-28	108.70	C14-C16-O73	107.90	C26-C25-O71	112.30
C5-C6-31	109.80	C17-C15-H57	122.50	C25-C26-H48	108.20
C7-C5-C19	108.90	C15-C17-H55	113.50	C25-C26-H49	111.50
C5-C7-C9	109.90	C15-C17-H56	113.50	C25-C26-O74	107.00
C5-C7-C10	114.80	C15-C17-O73	104.30	H50-C25-O71	103.40
C5-C7-H32	104.40	H67-C16-O73	122.40	H48-C26-H49	108.30
C5-C19-H41	109.60	C16-H73-C17	108.80	H48-C26-O74	110.40
C5-C19-H42	112.50	H55-C17-H56	109.10	H49-C26-O74	111.50
C5-C19-H43	112.40	H55-C17-O73	108.10	C26-O74-H46	110.20
C11-C6-H28	108.90	H56-C17-O73	108.10	H45-O69-H47	121.00
				O68-H47-O69	140.20

TABLE-3
FT-IR FUNCTIONAL GROUP
INTERPRETATIONS OF THE NAG MOLECULE

Literature	Theoretical	Experimental frequency (cm^{-1})	Functional groups interpretations of NAG
3437	3486	3449	(-OH group)
2934	2993	2940	(=CH stretch)
2840	2839	2847	(–CH_3 asymmetric stretch)
1748	1738	1609	(Carbonyl group C=O stretching band)
1443	1472	1457	(=CH double bond)
1354	1345	1353	(–CH_2 bending vibration)
908	937	910	(–CH_2 bending vibration)

double bond, which was found at 1457 cm^{-1}. The -CH_2 bending vibration experimental peaks shows the fingerprint region are at 1353 and 910 cm^{-1}. Several investigators have employed FTIR studies to confirm the NAG molecule, essential groups. The FTIR spectra signals were comparable to the FTIR spectrum of the standard NAG. The attributions of these bands can be verified in the studies reported by Singh *et al*. [30], who obtained these modes of vibration in comparatively nearby bands after evaluating the NAG component.

Mass spectrum studies: The molecular weight of 480.59 (MH^+) was known using HRMS spectrometry and the molecular ion peak was found to be a water molecule at *m/z* 498.56 $(M+H+H_2O)^+$.

^{1}H NMR spectrum: With TMS acting as an internal reference at 500 MHz, the observational spectrum data for the title molecule in DMSO are shown in Table-4. Basically, the B3LYP/GIAO was used to plan the absolute isotropic compound shielding [31]. Then, used the equivalent TMS shielding: $\sigma_{calc.}$(TMS) computed previous identical theoretical level as this work, relative chemical shifts were evaluated. Composed with computed values of $\sigma_{calc.}$(TMS), with computed standards of $\sigma_{calc.}$(TMS), mathematical values of chemical shift $\delta_{calc} = \sigma_{calc.}(TMS) - \sigma_{calc.}$ are obtained in Table-4, demonstrated the chemical shift by ^{1}H NMR experimental. Consequently, the study revealed experimental data for the identified compound NAG and the expected proton chemical shifts were in excellent agreement.

Mulliken atomic charges: The Mulliken atomic charges are greatly influenced using concept of atoms. The atomic charges are required for quantum chemical calculations in the molecular system since they have an influence on a wide variety of system properties. With DFT/B3LYP/6-311++G (d,p) basis set used to compute the Mulliken atomic charges. At the DFT level, NAG has the biggest positive charge on the C20 carbon, measuring 0.277. Given the increased negative charges DFT level on NAG's C19 carbon and O74 oxygen were -0.514 and -0.598, correspondingly. There is a positive charge on every hydrogen.

Frontier molecular orbital energies: Low FMOs energy gap chemical molecules frequently exhibit higher chemical reactivity and lower kinetic stability. The HOMO orbitals have clustered around trimethyl-6-methylenedeca hydronaphthalene and the LUMO orbitals have stretched toward the furan-2(5*H*)-one moiety in the isolated molecule NAG. This explains the charge transfer interaction between the furan-2(5*H*)-one molecule and trimethyl-6-methylenedecahydronaphthalene. Since they regulate whether molecules react to other species, the HOMO and LUMO are essential [32,33]. An electron is less likely to be excited from HOMO to LUMO when there is large gap, which could lower the inhibitor's affinity for the target protein. As a result, the band gap of NAG compound is less [34]. The calculative quantum chemical parameters of HOMO-LUMO for NAG are given in Table-5 and the HOMO-LUMO charge density map for the reference molecule (NAG) is displayed in Fig. 4.

Molecular electrostatic potential: The molecular electrostatic potential (MEP) plot of NAG may be shown with colour label order from +0.07319 a.u. (dark blue) to -0.07319 a.u. (dark

TABLE-4
EXPERIMENTAL AND CALCULATED
^{1}H NMR PARAMETERS (WITH RESPECT TO TMS)

Proton	σ_{TMS}	B3LYP/6-31G σ_{calc}	σ_{calc} (σ_{TMS} – σ_{calc})	Exp. δ (ppm)
H27	33.5426	27.75	4.84	4.8
H28	–	31.56	1.03	1.01
H29	–	30.69	1.91	–
H30	–	31.70	0.89	0.95
H31	–	30.89	1.70	–
H32	–	30.99	1.61	1.61
H33	–	31.00	1.60	1.51
H34	–	31.35	1.25	1.21
H35	–	27.81	4.78	4.79
H36	–	28.18	4.41	4.59
H37	–	31.41	1.19	–
H38	–	31.48	1.12	–
H39	–	32.29	0.61	0.63
H40	–	31.29	1.31	–
H41	–	32.26	0.34	–
H42	–	31.57	1.02	–
H43	–	31.77	0.83	–
H44	–	32.15	0.44	–
H45	–	30.03	2.57	2.36
H46	–	32.32	0.28	–
H47	–	28.59	4.00	3.62
H48	–	29.29	3.31	3.09
H49	–	28.35	4.25	4.38
H50	–	27.84	4.76	4.86
H51	–	29.50	3.09	3.03
H52	–	28.53	4.07	4.03
H53	–	28.68	3.92	3.43
H54	–	27.62	4.97	4.85
H55	–	28.02	4.58	4.83
H56	–	28.01	4.59	4.81
H57	–	25.99	7.59	7.48
H58	–	30.28	2.32	2.33
H59	–	30.75	1.85	1.71
H60	–	30.47	2.13	–
H61	–	30.54	2.05	–
H62	–	30.59	2.01	–
H63	–	31.30	1.30	–
H64	–	31.09	1.50	1.64
H65	–	31.21	1.39	–
H66	–	29.38	3.22	3.07

TABLE-5
CALCULATED QUANTUM CHEMICAL PARAMETERS HOMO-LUMO RESULTS OF NEOANDROGRAPHOLIDE VALUES

Quantum parameters (eV)	NAG (HOMO-LUMO)
E_{HOMO}	-6.778
E_{LUMO}	-4.169
ΔE_{gap}	2.609
$I = -E_{HOMO}$	6.778
$A = -E_{LUMO}$	4.169
$\chi = \frac{I+A}{2}$	5.474
$\mu = -\frac{I+A}{2}$	-5.474
$\eta = \frac{I-A}{2}$	1.035
$S = \frac{1}{2\eta}$	0.6525
$\omega = \frac{\mu^2}{2\eta}$	7.144

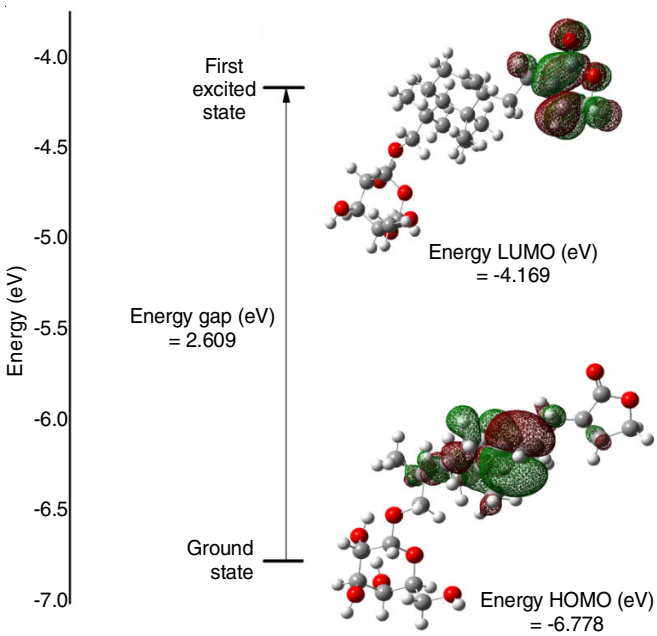

Fig. 4. Molecular orbital energy level diagram with HOMO and LUMO orbital of neoandrographolide

red) (Fig. 5). Positive areas were observed above the protonated 6-(hydroxymethyl)tetrahydro-2*H*-pyran group in the MEP of NAG. The hostile areas cover the furan-2(5*H*)-one group containing electronegative oxygen atoms. The carbon atom of the isolated NAG molecule is located on the MEP surfaces with zero potential in the green region. MEP is the potential, situated halfway is the potential, situated halfway among the two utmost of the deepest red and blue colours.

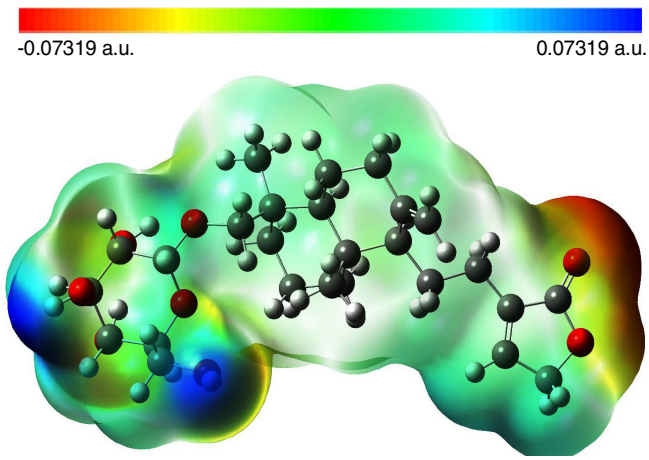

Fig. 5. Molecular electrostatic potential (MEP) of neoandrographolide

Antibacterial studies: The compound NAG from the powdered formulation demonstrated with effective antibacterial studies against Gram-positive and Gram-negative microorganisms, utilized streptomycin as a positive control. At 0.5 g/mL, the isolated NAG demonstrated significant bactericidal action in contradiction of *Staphylococcus aureus* (MTCC 3615), with a maximal inhibition zone is 17.3 ± 1.0 mm and a least zone of inhibition of 10.6 ± 0.5 mm against *Enterococcus faecalis* (MTCC 439) (Table-6).

TABLE-6
ANTIBACTERIAL ACTIVITY OF NEOANDROGRAPHOLIDE AGAINST GRAM-POSITIVE AND GRAM-NEGATIVE BACTERIA

Organisms	Streptomycin (mm)	Antibacterial activity (mm)				
		0.5 µg/mL	1 µg/mL	1.5 µg/mL	2 µg/mL	2.5 µg/mL
Staphylococcus aureus (MTTC 3615)	20.1 ± 1.0	12.0 ± 0.1	13.6 ± 0.2	14.3 ± 0.5	16.0 ± 1.1	17.3 ± 1.0
Enterococcus faecalis (MTCC 439)	19.3 ± 0.5	10.6 ± 0.5	11.0 ± 1.0	12.6 ± 1.0	14.3 ± 0.5	16.0 ± 1.1
Yersinia enterocolitica (MTCC 840)	21.3 ± 0.5	11.6 ± 0.5	11.0 ± 0.5	11.6 ± 0.5	13.3 ± 1.0	14.6 ± 1.0
Proteus mirabilis (MTCC 1771)	20.1 ± 0.5	12.6 ± 0.5	13.3 ± 0.5	14.3 ± 1.0	15.3 ± 1.0	16.0 ± 1.0

In vitro antioxidant study

Hydrogen peroxide scavenging activity: Compound NAG was also evaluated for its ability to scavenge H_2O_2 and at concentrations of 1000 µg/mL, respectively, it exposed an extreme scavenging property of 72.1 ± 1.3% ($p < 0.05$). Fig. 6 illustrates the hydrogen peroxide scavenging capabilities of the compound NAG.

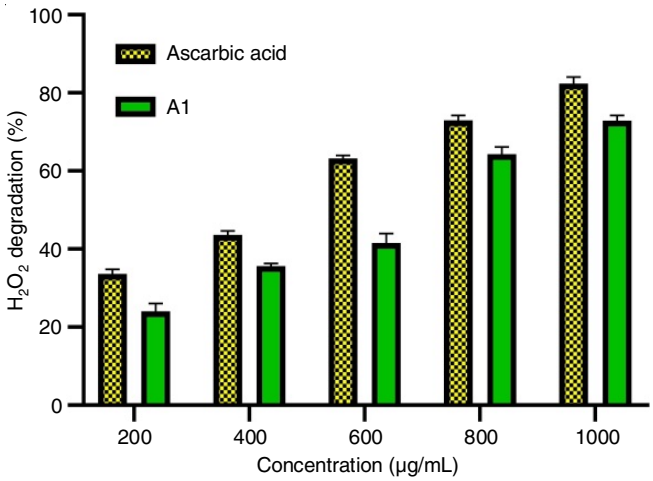

Fig. 6. Hydrogen peroxide scavenging property of changed concentrations (200-1000 µg/mL) of neoandrographolide and ascorbic acid (values are mean ± SD)

α-Amylase assay: This was done to plot the percentage of α-amylase inhibition depending on sample concentrations and IC_{50} values (Fig. 7). The reference drug (acarbose) was exhibited to posses an IC_{50} value of 23.4009 µg/mL, while the IC_{50} value of NAG was 33.2769 µg/mL. The IC_{50} values for acarbose and the sample did not significantly differ.

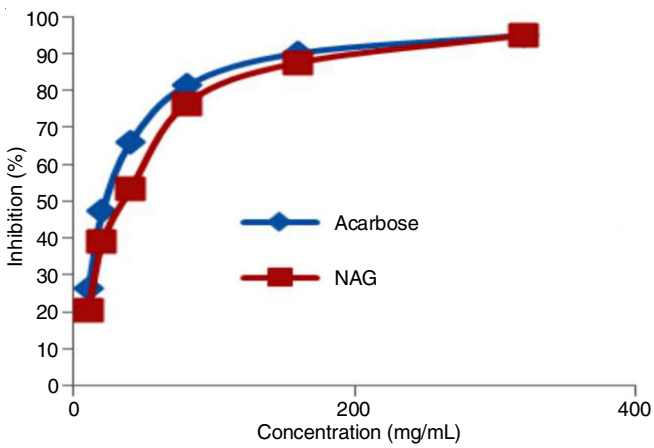

Fig. 7. α-Amylase inhibitory assay of neoandrographolide

***In silico* molecular docking:** This work aimed to design of the mitotic control 2 (MAD2) interface for FAT10 before examining the effects of disturbed FAT10-MAD2 interaction on the growth of FAT10-induced tumors. A proteasome degradation signal-interacting ubiquitin modification protein is called FAT10 [35-37]. The thymus and spleen are two immune system tissues where FAT10 is primarily expressed. The occurrences have a tight connection to tumorigenesis, which is a defining feature of many solid tumors. There is no clear understanding of the process at this time. FAT10 underlies this. It has been discovered as proof that FAT10 interrelates with the protein that causes mitotic arrest-deficiency 2 (MAD2) through mitosis in spindles. This connection prevents MAD2 from localizing to the kinetochores, which causes aneuploidy [38,39].

The inhibition constant (ki) and the binding affinity for NAG are exposed in Table-7. The results recommend that the NAG ligand may significantly occupy the active site of (PDB ID: 2MBE) through residue interaction. A range of bond lengths and binding types are displayed in Table-8. Figs. 8-10 display the 2D interactions, inhibition constant (ki) indicates ligand-enzyme interaction has reached its conclusion. Less medicine will be required to block the activity of that enzyme if ki is lower. These findings demonstrate the interaction among the protein (PDB code: 2MBE), NAG ligand. Its inhibition constant (ki) value is 3.3397 µM and its reduced binding energy value is -6.1 (Kcal/mol).

TABLE-7
AUTO DOCK VINA RESULTS OF THE BINDING AFFINITY AND RMSD VALUES OF DIFFERENT POSES IN 2MBE INHIBITOR OF NEOANDROGRAPHOLIDE

Mode	NAG-2MBE		
	Affinity (kcal/mol)	rmsdl.b.	rmsdu.b
1	-6.1	0	0
2	-6.1	2.332	3.093
3	-6	18.731	21.119
4	-5.6	19.757	22.961
5	-5.6	13.487	15.93
6	-5.6	4.636	7.621
7	-5.4	5.217	7.815
8	-5.3	6.684	10.241
9	-5.1	19.349	22.831
Inhibition constant: 3.3397 µM			

Conclusion

The isolated compound neoandrographolide (NAG) from ethanolic extract of Nilavembu Kudineer Chooranam (NKC), a traditional Siddha medicine powder, was analyzed with FT-IR, mass and NMR spectroscopy techniques in addition to TLC and chemical structural interpretation. The GC-MS study of

TABLE-8
THE LIGAND-RECEPTOR RESIDUE INTERACTION BETWEEN NEOANDROGRAPHOLIDE WITH 2MBE PROTEIN

Pub chem. Id	Ligand name	Residue interaction	Type of bond	Distance (Å)
2MBE	NAG	: UNK0:H-A: GLN41:O	Hydrogen	2.58
		: UNK0:H-A: LYS25:O	Hydrogen	2.82
		A: HIS29: C-:UNK0:O	Hydrogen	3.12
		A: TRP10-:UNK0	π-Alkyl hydrophibic	5.42

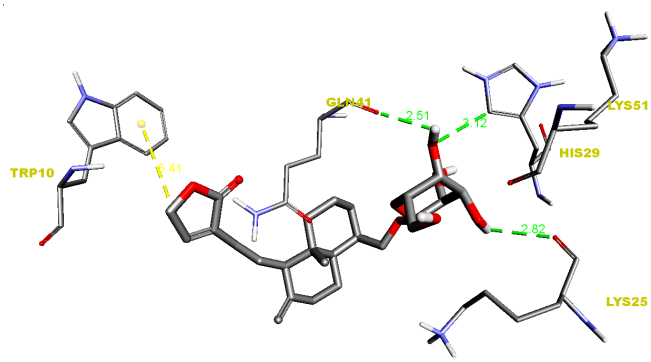

Fig. 8. Hydrogen bond interaction of neoandrographolide with 2MBE protein

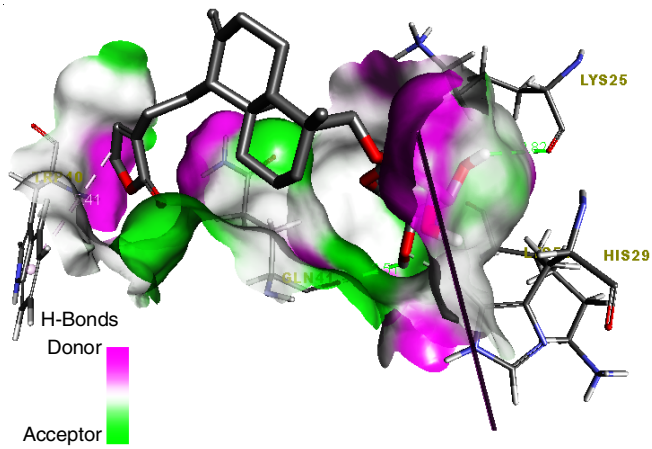

Fig. 9. Hydrogen bond receptor-side surface interaction of neoandrographolide with 2MBE protein

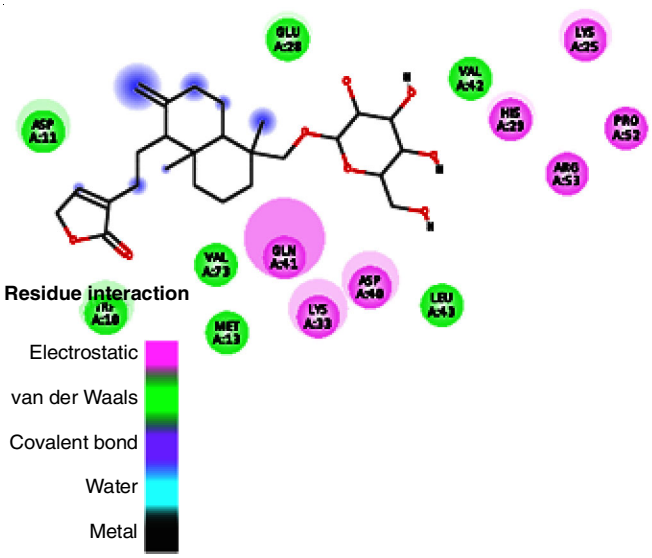

Fig. 10. 2D-Hydrogen bond interaction representation of NAG ligand with 2MBE protein

an ethanolic extract of NKC revealed that it had the therapeutic value of phytochemical ingredients such as piperidine, 1-(piperidin-1-yl)dodecan-1-one, 1-(1-oxo-9-octadecenyl)piperidine, 1-acetyl-, butan-2-one, 4-(3-hydroxy-2-methoxyphenyl)- and the continuing were less than 6%. The FT-IR spectrum exhibited the peaks demonstrating the occurrence of -OH group, =CH stretch and $–CH_3$ asymmetric stretch, C=O stretching band, =CH double bond, the fingerprint region $–CH_2$ bending vibra-tion were determined successfully and these values well agree with the theoretical and literature survey. High-resolution mass spectrometry revealed the molecular ion peak as adduct form-ation with water molecules at *m/z* 498.56 ($M+H+H_2O$). Olefinic protons of the unsaturated lactone system were found at 7.47 ppm in the ^1H NMR spectrum. The C-14 proton resonated as two singlets at δ 4.79 and 4.86. The signals for the two *tert.*-methyl groups appeared at δ 0.61 (C-13) and 0.95 (C-11). Acid hydrolysis, followed by paper chromatography, confirmed the presence of sugar moiety. Biological results from the α-amylase analysis suggest that NAG has an excellent α-amylase inhibitor activity. *In vitro* antibacterial and antioxidant studies have been carried out and excellent results have been evaluated. An *in silico* study revealed that the protein (PDB code: 2MBE) interacts with the NAG ligand have the value of -6.1 (Kcal/mol) and ki value of 3.3397 μM. Therefore, it provides a theoretical foundation for the analysis of compounds with structures similar to NAG that exhibit physiological activity, however, whose complete biological effects remain inadequately understood by existing experimental methodologies.

CONFLICT OF INTEREST

The authors declare that there is no conflict of interests regarding the publication of this article.

REFERENCES

1. P. Mekala and T.R.G.K. Murthy, *J. Pharmacogn. Phytochem.*, **9**, 1031 (2020); https://doi.org/10.22271/phyto.2020.v9.i3q.11428
2. A.H. Gilani and Atta-ur-Rahman, *J. Ethnopharmacol.*, **100**, 43 (2005); https://doi.org/10.1016/j.jep.2005.06.001
3. I. Giannenas, E. Sidiropoulou, E. Bonos, E. Christaki and P. Florou-Paneri, *Phytomed. Plus*, **1**, 100029 (2021); https://doi.org/10.1016/j.phyplu.2021.100029
4. K. Anbarasu, K.K. Manisenthil and S. Ramachandran, *Asian Pac. J. Trop. Med.*, **4**, 819 (2011); https://doi.org/10.1016/S1995-7645(11)60201-0
5. T. Yang, H.-X. Shi, Z.-T. Wang and C.-H. Wang, *Planta Med.*, **76**, 1698 (2010); https://doi.org/10.1055/s-0030-1249876
6. P.H. Pfisterer, J.M. Rollinger, L. Schyschka, A. Rudy, A.M. Vollmar and H. Stuppner, *Planta Med.*, **76**, 1698 (2010); https://doi.org/10.1055/s-0030-1249876
7. T. Yang, H. Shi, Z. Wang and C. Wang, *Phytother. Res.*, **27**, 618 (2013); https://doi.org/10.1002/ptr.4771

8. J. Liu, Z.-T. Wang and L.-L. Ji, *Am. J. Chin. Med.*, **35**, 317 (2007); https://doi.org/10.1142/S0192415X07004849
9. S.P. Adiguna, J.A. Panggabean, A. Atikana, F. Untari, F. Izzati, A. Bayu, A. Rosyidah, S.I. Rahmawati and M.Y. Putra, *Pharmaceuticals*, **14**, 1102 (2021); https://doi.org/10.3390/ph14111102
10. Y. Koteswara Rao, G. Vimalamma, C. Venkata Rao and Y.-M. Tzeng, *Phytochemistry*, **65**, 2317 (2004); https://doi.org/10.1016/j.phytochem.2004.05.008
11. G.R. Mallavarapu, K.V. Syamasundar, S. Ramesh and B.R.R. Rao, *Nat. Prod. Commun.*, **7**, 223 (2012); https://doi.org/10.1177/1934578X1200700228
12. J.G. Millar, *J. Nat. Prod.*, **61**, 1025 (1998); https://doi.org/10.1021/np9800699
13. Y. Matsuo and Y. Mimaki, *Phytochemistry*, **77**, 304 (2012); https://doi.org/10.1016/j.phytochem.2012.02.007
14. C.K. Kokate, Preliminary Phytochemical Analysis, Practical Pharmacognosy, Vallabh Prakashan: New Delhi, edn. 1 (1986).
15. P. Kamalarajan, S. Muthuraman, M.R. Ganesh and M.F. Valan, *European J. Med. Plants*, **30**, 1 (2020); https://doi.org/10.9734/ejmp/2019/v30i430187
16. H. Wang, L. Guo, H. Zuo, L. Wang, X. Guo, Z. Kang, Z.Y. Li, L. Jiao and E. Hao, *Eur. J. Org. Chem.*, **27**, e202400660 (2024); https://doi.org/10.1002/ejoc.202400660
17. J.I. Ahamed, F. K, A.V. Priya, J. Prema Kumari, P. Kamalarajan, R.P. Steiny and B. Venkatadri, *J. Mol. Struct.*, **1252**, 132186 (2022); https://doi.org/10.1016/j.molstruc.2021.132186
18. J.I. Ahamed, G.R. Ramkumaar, P. Kamalarajan, K. Narendran, M.F. Valan, T. Sundareswaran, T.A. Sundaravadivel, B. Venkatadri and S. Bharathi, *J. Mol. Struct.*, **1248**, 131418 (2022); https://doi.org/10.1016/j.molstruc.2021.131418
19. H.B. Schlegel, *J. Comput. Chem.*, **3**, 214 (1982); https://doi.org/10.1002/jcc.540030212
20. N. Subramanian, N. Sundaraganesan, S. Sudha, V. Aroulmoji, G.D. Sockalingam and M. Bergamin, *Spectrochim. Acta A Mol. Biomol. Spectrosc.*, **78**, 1058 (2011); https://doi.org/10.1016/j.saa.2010.12.049
21. J.I. Ahamed, M.F. Valan, K. Pandurengan, P. Agastian, B. Venkatadri, M.R. Rameshkumar and K. Narendran, *Res. Chem. Intermed.*, **47**, 759 (2021); https://doi.org/10.1007/s11164-020-04297-3
22. J. Foresman and E. Frish, Exploring Chemistry with Electronic Structure Methods, Gaussian Inc., Pittsburgh. edn. (1996).
23. P.J. Hay and W.R. Wadt, *J. Chem. Phys.*, **82**, 270 (1985); https://doi.org/10.1063/1.448799
24. J. Zhao, Y. Zhang and L. Zhu, *J. Mol. Struct. THEOCHEM*, **671**, 179 (2004); https://doi.org/10.1016/j.theochem.2003.10.065
25. R. Ditchfield, *J. Chem. Phys.*, **56**, 5688 (1972); https://doi.org/10.1063/1.1677088
26. R.J. Ruch, S.J. Cheng and J.E. Klaunig, *Carcinogenesis*, **10**, 1003 (1989); https://doi.org/10.1093/carcin/10.6.1003
27. B. Venkatadri, A. Khusro, C. Aarti, M.R. Rameshkumar and P. Agastian, *Asian Pac. J. Trop. Biomed.*, **7**, 782 (2017); https://doi.org/10.1016/j.apjtb.2017.08.003
28. G.M. Morris, D.S. Goodsell, R.S. Halliday, R. Huey, W.E. Hart, R.K. Belew and A.J. Olson, *J. Comput. Chem.*, **19**, 1639 (1998); https://doi.org/10.1002/(SICI)1096-987X(19981115)19:14<1639::AID-JCC10>3.0.CO;2-B
29. BIOVIA Discovery Studio Visualizer, Accelrys Software Inc. Discovery Studio Visualizer (2005).
30. P.K. Singh, T. Hasan and N. Misra, *J. Chem.*, **6**, 183 (2009); https://doi.org/10.1155/2009/369569
31. K. Wolinski, J.F. Hinton and P. Pulay, *J. Am. Chem. Soc.*, **112**, 8251 (1990); https://doi.org/10.1021/ja00179a005
32. A. Rauk, Orbital Interaction Theory of Organic Chemistry. John Wiley & Sons, edn. 2 (2004).
33. A. Teimouri, A.N. Chermahini, K. Taban and H.A. Dabbagh, *Spectrochim. Acta A Mol. Biomol. Spectrosc.*, **72**, 369 (2009); https://doi.org/10.1016/j.saa.2008.10.006
34. E. Eroglu and H. Türkmen, *J. Mol. Graph. Model.*, **26**, 701 (2007); https://doi.org/10.1016/j.jmgm.2007.03.015
35. G. Schmidtke, B. Kalveram and M. Groettrup, *FEBS Lett.*, **583**, 591 (2009); https://doi.org/10.1016/j.febslet.2009.01.006
36. N. Rani, A. Aichem, G. Schmidtke, S.G. Kreft and M. Groettrup, *Nat. Commun.*, **3**, (2012); https://doi.org/10.1038/ncomms1752
37. M.S. Hipp, B. Kalveram, S. Raasi, M. Groettrup and G. Schmidtke, *Mol. Cell. Biol.*, **25**, 3483 (2005); https://doi.org/10.1128/MCB.25.9.3483-3491.2005
38. Y.C. Liu, J. Pan, C. Zhang, W. Fan, M. Collinge, J.R. Bender and S.M. Weissman, *Proc. Natl. Acad. Sci. USA*, **96**, 4313 (1999); https://doi.org/10.1073/pnas.96.8.4313
39. C.G.L. Lee, J. Ren, I.S.Y. Cheong, K.H.K. Ban, L.L.P.J. Ooi, S. Yong Tan, A. Kan, I. Nuchprayoon, R. Jin, K.-H. Lee, M. Choti and L.A. Lee, *Oncogene*, **22**, 2592 (2003); https://doi.org/10.1038/sj.onc.1206337